Available online at www.sciencedirect.com
ScienceDirect
Trans. Nonferrous Met. Soc. China 34(2024) 655−668
Transactions of Nonferrous Metals Society of China
www.tnmsc.cn

Influencing mechanism of visible light and silver ions on p- and n-type chalcopyrite bioleaching

Chun-xiao ZHAO, Jun WANG, Yang LIU, Rui LIAO, Bao-jun YANG, Guan-zhou QIU

Key Laboratory of Biohydrometallurgy, Ministry of Education, School of Minerals Processing and Bioengineering, Central South University, Changsha 410083, China

Received 20 September 2022; accepted 22 March 2023

Abstract: Different effects and mechanisms of visible light and silver ions (Ag^+) on the bioleaching of p- and n-type chalcopyrite (Cpy A and Cpy B, respectively) in the presence of *Acidithiobacillus ferrooxidans* were investigated. The semiconductor characteristics, bioleaching behaviors, surface morphologies, main phases and surface species of chalcopyrite were evaluated by Hall effect test, bioleaching tests, X-ray diffraction, scanning electron microscope and X-ray photoelectron spectroscopy. According to the results, Cpy A had a higher carrier concentration and greater carrier mobility than Cpy B, resulting in a faster dissolution rate. After 24 d of bioleaching, the copper extraction rate of Cpy A was 91.05%, which was 17.86% higher than that of Cpy B (73.19%) when light illumination and Ag^+ existed together. Obviously, visible light and Ag^+ promoted the bio-dissolution process of Cpy A more strongly than Cpy B, which was mainly attributed to the higher carrier mobility in Cpy A. Furthermore, charge transfer occurred more rapidly on the chalcopyrite surface when illuminated, and more Ag_2S was accumulated, especially for Cpy A. As a result, the dense structure of the passivation layer was destroyed, reducing the passivation effect and promoting chalcopyrite dissolution.
Key words: *Acidithiobacillus ferrooxidans*; Hall effect; semiconductor characteristics; light illumination; chalcopyrite; bioleaching

1 Introduction

Copper is widely applied in machinery, construction, electronics and other industries for its excellent physical properties [1]. Chalcopyrite, making up approximately 70% of copper reserves in the world, is the most abundant of copper sulfides [2]. At present, chalcopyrite is mainly investigated by traditional pyrometallurgical methods. However, these methods emit SO_2, causing air pollution, and the operation cost is high. With the growing global environmental awareness and the depletion of copper resources, bioleaching was proposed as an economical and efficient low-grade copper ore processing technology [3]. Actually, it has been applied successfully to extracting valuable metals such as uranium, zinc and copper from low-grade ores [4]. However, efficient chalcopyrite dissolution is challenging because of the high lattice energy and the generation of passivation layers like elemental sulfur, poly-sulfides, jarosite, and metal-deficient sulfide [5,6]. Accordingly, it is necessary to understand chalcopyrite bioleaching mechanisms and influences to increase its extraction rate.

To date, researchers have explored the effects of various factors (e.g., temperature [7], microorganism types [8], metal ions [9] and pH values [10]) on chalcopyrite bioleaching. By studying various acidophilic bacteria, it can be concluded that *Acidithiobacillus ferrooxidans* (*A. ferrooxidans*) has iron- and sulfur-oxidizing abilities, and plays an important role in chalcopyrite

Corresponding author: Bao-jun YANG, Tel: +86-13974885694, E-mail: yangbaojun0312@126.com
DOI: 10.1016/S1003-6326(23)66425-8

bioleaching [11,12]. In addition, Ag^+ exhibits excellent catalytic properties [13]. Generally speaking, there are three types of the mechanisms of Ag^+-catalyzed chalcopyrite leaching: (1) a direct reaction between Ag^+ and chalcopyrite produces Ag_2S, which induces a porous sulfur film to form instead of an impervious elemental sulfur layer (Reaction (1)) [14], (2) Ag^+ changes the morphology and enhances the conductivity of chalcopyrite by introducing Ag_2S or Ag^0 into the passivation film (Reactions (2) and (3)) [15], and (3) Ag^+ is trapped on the surface of chalcopyrite to form Ag_2S and generates sulfur vacancies and holes, leading to the formation of a porous sulfur film and the fast diffusion rate [16]. However, the specific mechanism is still controversial, which may be related to the diversity of chalcopyrite samples, such as electronic structures and semiconductor properties.

$$CuFeS_2+4Ag^+=Cu^{2+}+Fe^{2+}+2Ag_2S \quad (1)$$

$$2CuFeS_2+6H^++2e=Cu_2S+2Fe^{2+}+3H_2S \quad (2)$$

$$H_2S+2Ag^+=2H^++Ag_2S \quad (3)$$

It is reported that chalcopyrite is a semiconductor with a band gap of 0.6 eV [17], which can be divided into p- and n-type according to the level and kind of doping [18,19]. The Hall effect has been used to determine the semiconductor type of chalcopyrite [20]. With the help of the Hall coefficient (R_H), the type of carriers present in the semiconductor sample can be determined [21]. If the R_H is positive, the chalcopyrite is a p-type semiconductor in which the main charge carriers are holes, and if it is negative, the chalcopyrite is an n-type semiconductor in which the main charge carriers are electrons [22]. When irradiated with energy ($h\nu$) greater than or equal to its band gap energy, charge carriers (electron (e)−hole (h) pair) are generated and then migrate to the chalcopyrite surface (Reaction (4)), promoting the redox reaction [23]. And chalcopyrite bioleaching is a redox dissolution process. CRUNDWELL et al [24] have shown that visible light can promote the dissolution of the chalcopyrite. A similar result was reported by ZHOU et al [25] who found that the dissolved copper in the shake flask with 8500 lux light was 91.80% higher than that without light. In another study, YEPSEN et al [23] have proposed that visible light induced photo-leaching of copper from chalcopyrite and achieved yields close to 3% within 4 h. Additionally, visible light is ubiquitous in nature. Based on the above theory, the synergistic promotion of visible light and Ag^+ on chalcopyrite bioleaching has been explored [26]. What is more, p-type chalcopyrite was more easily corroded by microorganisms than n-type chalcopyrite [20]. However, as far as we know, the difference of chalcopyrite with different semiconductor types in response to visible light and Ag^+ has not been investigated.

$$CuFeS_2+h\nu \rightarrow CuFeS_2(e+h) \quad (4)$$

Hence, different effects of n- and p-type chalcopyrite in response to light illumination and Ag^+ mediated by *A. ferrooxidans* were investigated in this work. The semiconductor characteristic of chalcopyrite was determined through the Hall effect measurement. The mineral phase changes after chalcopyrite bioleaching, the surface morphologies of leached residues, and the evolutions of Ag, Cu, S and O in the bioleaching process were studied as well in order to know the mechanism of chalcopyrite bioleaching. In light of these analyses, a model was established to investigate the mechanism of p- and n-type chalcopyrite in the presence of visible light and Ag^+, and to improve the bioleaching rate of chalcopyrite.

2 Experimental

2.1 Characteristics and compositions of chalcopyrite samples

Two chalcopyrite samples (Cpy A and Cpy B), obtained from the Chambishi Copper Mine in Zambia and Yunnan Province of China, respectively, were used in this work. Mineral samples were ground and sieved to be less than 74 μm, and then stored in the vacuum drying oven [27]. Impurities were removed from the samples by ultrasonic cleaning for 5 min [19]. Copper contents of Cpy A and Cpy B were 34.39 wt.% and 31.77 wt.%, respectively, detected by chemical analysis (iodometric titration) [28]. Based on these values, copper extraction rates were calculated. The X-ray diffraction (XRD) analysis revealed that Cpy A had only the diffraction peaks of chalcopyrite, while Cpy B was dominated by chalcopyrite followed by trace amounts of pyrite and quartz (Fig. 1). X-ray fluorescence (XRF) analysis results displayed that Cpy A mainly contained Cu (35.49 wt.%), Fe

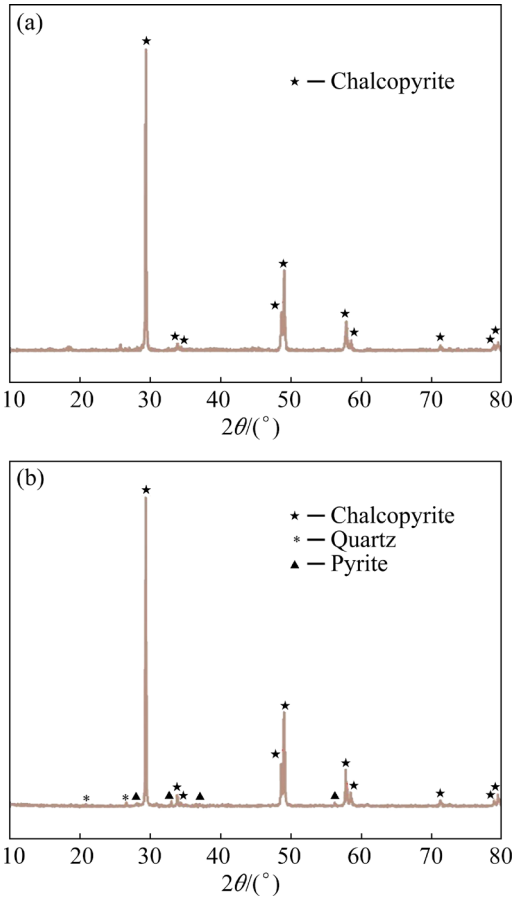

Fig. 1 XRD patterns of original Cpy A (a) and Cpy B (b) samples

(30.17 wt.%), S (30.95 wt.%), and Cpy B was mostly composed of Cu (33.89 wt.%), Fe (30.31 wt.%), and S (29.33 wt.%).

The Hall effect was studied to determine the semiconductor types of two chalcopyrite samples (Table 1) [21]. With the help of the Hall coefficient R_H, Cpy A was determined as p-type chalcopyrite whose main carriers were holes (R_H was positive), and Cpy B was identified as n-type chalcopyrite whose primary carriers were electrons (R_H was negative) [22]. Moreover, the carrier concentration of Cpy A (1.61×10^{16} cm^{-3}) was higher than that of Cpy B (1.48×10^{16} cm^{-3}), and the resistivity of Cpy A (7.94 Ω·cm) was lower than that of Cpy B (60.1 Ω·cm). Additionally, the carrier mobility of Cpy A was 22.4 cm^2/(V·s), which was significantly higher than that of Cpy B (2.55 cm^2/(V·s)).

2.2 Microorganisms and culture medium

A. ferrooxidans (ATCC 23270, obtained from the Key Lab of Biohydrometallurgy, Ministry of Education, Central South University) was cultivated to mid-exponential phase in the 9K medium at 30 °C with shaking at 170 r/min. The 9K medium consisted of $(NH_4)_2SO_4$ 3 g/L, KCl 0.1 g/L, $K_2HPO_4\cdot3H_2O$ 0.5 g/L, $MgSO_4\cdot7H_2O$ 0.5 g/L, $Ca(NO_3)_2$ 0.01 g/L and $FeSO_4\cdot7H_2O$ 44.7 g/L, and the initial pH was controlled at 2.0 with 0.01 mol/L H_2SO_4 [29]. Subsequently, bacteria suspensions were filtered through filter paper (Whatman 42) and centrifugated at 1×10^4 r/min and 4 °C for 15 min to obtain cell pellets after being triple subcultured [26]. Eventually, the harvested cell pellets were washed and dispersed in the iron-free 9K medium for subsequent experiments.

2.3 Bioleaching experiments

The bioleaching experiments were conducted in 250 mL Erlenmeyer flasks, which contained 100 mL of sterile basal medium and 2 g chalcopyrite. As *A. ferrooxidans* grew optimally at pH 2 [12], the initial pH value was controlled at 2.0 [30]. And the primary inoculum concentration of *A. ferrooxidans* was 2.0×10^7 cells/mL. Subsequently, all of the Erlenmeyer flasks were placed in a constant temperature illuminated shaker at 30 °C and 170 r/min and the light intensity was adjusted to 0 lux or 8500 lux since 8500 lux light could most effectively promote the dissolution of chalcopyrite [25]. Additionally, the bioleaching experiments were separated into 4 tests (T1−T4) and other experimental designs were shown in Table 2. The concentration of added Ag^+ (from Ag_2SO_4) was set to be 10 mg/L as this is the optimum concentration to promote chalcopyrite biodissolution [2]. Each experiment was repeated in triplicate to ensure the reliability of the results. During the bioleaching process, the sterile basal medium was periodically added for compensating

Table 1 Results of Hall effect analysis for two chalcopyrite samples

Sample	Carrier concentration/cm^{-3}	Mobility/(cm^2·V^{-1}·s^{-1})	Resistivity/(Ω·cm)	Hall coefficient, R_H/(cm^3·C^{-1})
Cpy A	1.61×10^{16}	22.4	7.94	1.16×10^4
Cpy B	1.48×10^{16}	2.55	60.1	-2.52×10^4

Table 2 Design of bioleaching experiments

Test No.	Condition
T1	Neither light illumination nor Ag^+ added
T2	Only 8500 lux light added without Ag^+
T3	Only 10 mg/L Ag^+ added without light illumination
T4	Both 8500 lux light and 10 mg/L Ag^+ added

sampling loss, and the evaporation loss was made up by adding deionized water. All chemicals used in experiments were of analytical grade.

2.4 Analysis techniques

During the bioleaching process, concentrations of copper ions (Cu^{2+}) were determined by the bis(cyclohexanone)oxalyldihydrazone spectrophotometry [31]. After the bioleaching experiments, solid residues were collected by filtering, rinsing and drying for subsequent analysis [29]. The surface morphologies and mineral phases of residues were detected by scanning electron microscope (SEM, Nova™ NanoSEM 230, FEI, USA) and XRD, separately. Besides that, the chemical species of Ag, Cu, S and O in the residues were analyzed by X-ray photoelectron spectroscopy (XPS) on a Thermo Fisher X-ray photoelectron spectrometer with the model of ESCALAB 250Xi. Due to the splitting of spin-orbits, the Ag 3d, Cu 2p and S 2p peaks all appeared as doublet peaks. For a clearer presentation, only the Ag $3d_{5/2}$, Cu $2p_{3/2}$ and S $2p_{3/2}$ peak were shown in the figures. All binding energies were calibrated by setting the peak of C 1s to be 284.6 eV [32]. And the background of spectra was obtained by the Shirley method.

3 Results and discussion

3.1 Effects of visible light and Ag^+ on chalcopyrite bioleaching

The changes in copper concentrations with time during chalcopyrite dissolution are shown in Fig. 2. Copper concentrations increased rapidly during the first 4 d of all tests. From day 4 to day 12, copper concentrations in T3 and T4 increased faster than those in T1 and T2. And the dissolution rate of

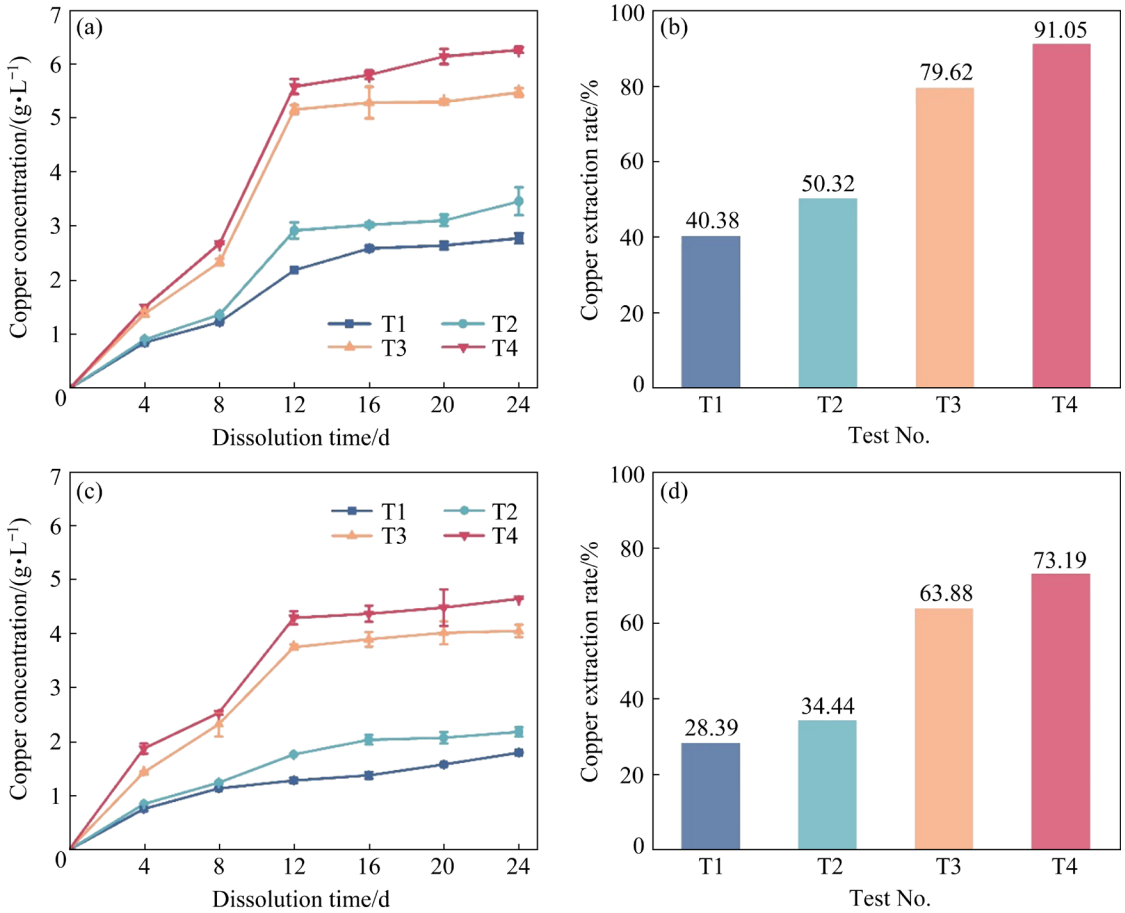

Fig. 2 Changes in copper concentrations of Cpy A (a) and Cpy B (c), and copper extraction rates of Cpy A (b) and Cpy B (d) after chalcopyrite bioleaching for 24 d in the presence of *A. ferrooxidans*

Cpy A was quicker than that of Cpy B. After 12 d, copper concentrations increased slowly in all tests, indicating that the chalcopyrite surface was passivated at this stage, which hindered the chalcopyrite bioleaching process. Finally, after bioleaching for 24 d, the bioleaching of chalcopyrite tended to stop in each test (Fig. 2(a)), the copper concentrations of Cpy A in different tests were (2.78±0.10) g/L (T1), (3.46±0.26) g/L (T2), (5.48±0.08) g/L (T3) and (6.26±0.05) g/L (T4), and the corresponding copper extraction rates were 40.38%, 50.32%, 79.62% and 91.05%, respectively. Meanwhile, for Cpy B, the concentrations of copper under different test conditions were (1.80±0.02) g/L (T1), (2.19±0.09) g/L (T2), (4.06±0.12) g/L (T3) and (4.65±0.01) g/L (T4), corresponding to the extraction rates of copper being 28.39%, 34.44%, 63.88% and 73.19%. Evidently, when illuminated, the extraction rates of Cpy A and Cpy B were increased by 9.94% and 6.05%, respectively. After adding Ag^+, the copper extraction rates of two chalcopyrite samples increased by 39.24% (Cpy A) and 35.49% (Cpy B), respectively. When light illumination and Ag^+ acted simultaneously, the final concentrations of copper released by Cpy A and Cpy B were the highest, which were increased by 50.67% and 44.80%, respectively. This indicated that the promotion effect of visible light and Ag^+ on the bioleaching of Cpy A was better than that of Cpy B, and visible light and Ag^+ possessed a synergistic effect. In addition, based on different semiconductor types, Cpy A (p-type chalcopyrite) was easier to dissolve than Cpy B (n-type chalcopyrite), even without additional light illumination and Ag^+. This finding was also consistent with previous studies [19,20]. LI and WANG [33] have reported that the initial reaction of chalcopyrite oxidation is the consumption of holes (h) (Reactions (5) and (6)), followed by electron transfer (Reactions (7) and (8)), resulting in Fe^{3+} in the conduction band and Cu^+ in the valence band. And according to the Hall effect analysis (Table 1), the carrier mobility of Cpy A was an order of magnitude higher than that of Cpy B. Therefore, the dissolution rate of p-type chalcopyrite was faster than that of n-type chalcopyrite.

$$CuFeS_2+3h=Fe^{3+}+CuS_2 \quad (5)$$

$$CuS_2+2h=Cu^{2+}+2S \quad (6)$$

$$CuS_2=Cu^{2+}+2S+2e \quad (7)$$

$$CuS_2=CuS+S \quad (8)$$

3.2 Changes in phase of leached residues

Figure 3 exhibits the crystal structure of leached chalcopyrite residues by XRD patterns. The analysis indicated that the main phase in the residues was chalcopyrite ($CuFeS_2$). For Cpy A, jarosite ($KFe_3(SO_4)_2(OH)_6$) appeared in the residues compared to the original chalcopyrite (Fig. 1(a)). And the added Ag^+ not only promoted the generation of jarosite but also led to the production of sulfur (S_8), especially under light illumination. Meanwhile, for Cpy B, compared with the initial chalcopyrite (Fig. 1(b)), the new phase of sulfur was formed in the residues only when Ag^+ was present. Although the main component in the residues was chalcopyrite in different bioleaching tests, the intensity of the T4 sample was significantly lower than that of the T1 sample. This

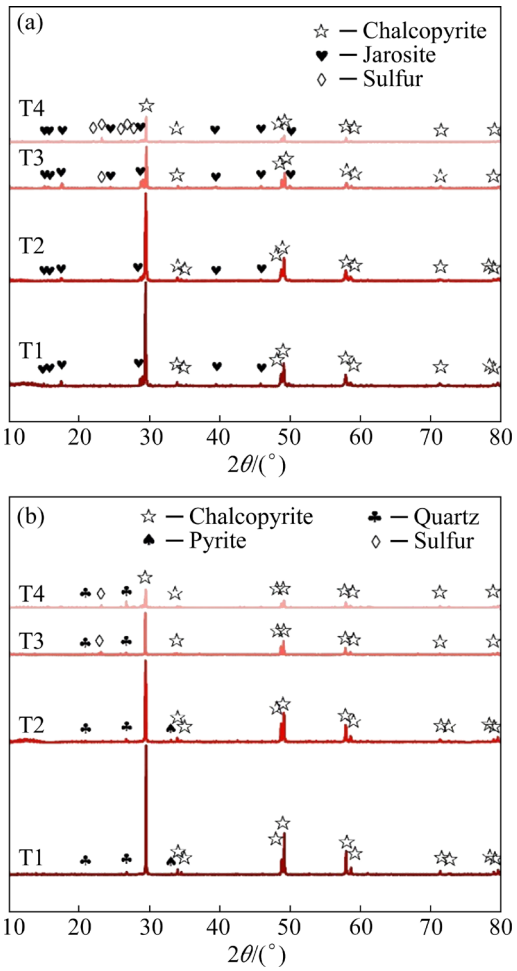

Fig. 3 XRD patterns of leached residues of Cpy A (a) and Cpy B (b)

meant that visible light and Ag^+ remarkably accelerated the dissolution of chalcopyrite, resulting in sulfur oxidation and substantial copper leaching. Moreover, the sulfur in Cpy A was oxidized more thoroughly and partially transformed into jarosite.

3.3 Surface species of chalcopyrite

XPS was used to reveal the chemical state changes of the two chalcopyrite samples surfaces after bioleaching. The changes of silver species, copper species, sulfur species and oxygen species on the surface of two chalcopyrite samples in the four tests were deeply analyzed (Figs. 4−7). And the content was correspondingly obtained by supposing that the percentages of various copper species, oxygen species and sulfur species were in proportion to the comprehensive areas under Cu 2p, O 1s and S 2p peaks, respectively [31].

3.3.1 XPS spectra of Ag 3d

Figure 4 exhibits the high-resolution XPS spectra of the Ag $3d_{5/2}$ region. Since Ag peaks were not discovered on the two chalcopyrite surfaces when no Ag^+ was added (T1 and T2), only the Ag $3d_{5/2}$ spectra of the chalcopyrite surface after adding Ag^+ were shown (T3 and T4). When Ag^+ was introduced separately, the Ag $3d_{5/2}$ spectra contained a peak at 367.7−368.0 eV, which was in good agreement with the published value of silver in Ag_2S compound [13,34]. Apparently, the peak intensities of the Ag-bearing phase increased with the addition of light illumination. For Cpy A, in the presence of both visible light and Ag^+, a new peak at 368.76 eV appeared, which was considered to be the typical peak of Ag^0 [35]. However, Ag_2S was still the main Ag-bearing component. This suggested that after the bioleaching process of chalcopyrite catalyzed by Ag^+, Ag_2S was formed on the surface of chalcopyrite residues and the reaction process can be illustrated as Reactions (1)−(3) [16,36]. Visible light significantly raised the content of Ag_2S on the surface of two chalcopyrite residues, and a small amount of Ag^0 was introduced on the surface of Cpy A. Therefore, another Ag^+-catalyzed reaction also occurred on the Cpy A surface during the simultaneous exposure to visible light and Ag^+, as is shown in Reaction (9) [13]. It has been reported that Ag_2S and/or Ag^0 formed on chalcopyrite surface can change the morphology, thereby weakening the effect of passivation and favoring the oxidation and dissolution of chalcopyrite [2].

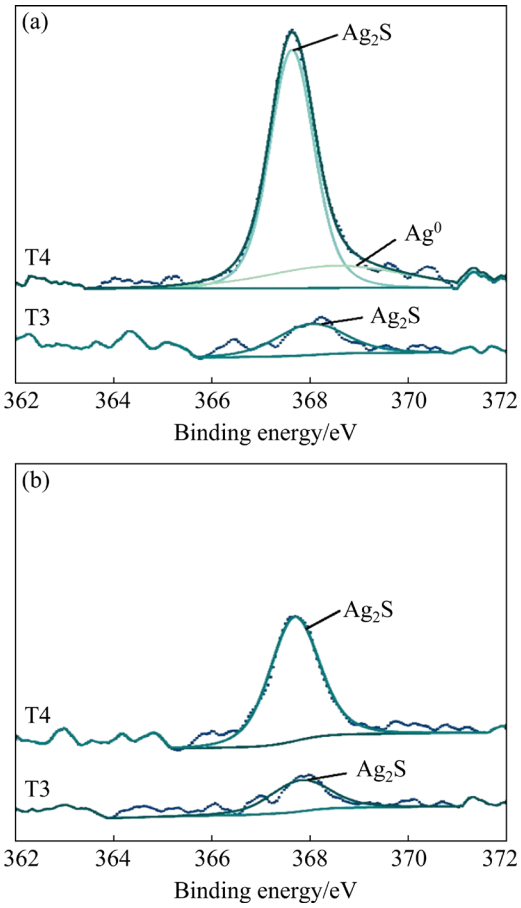

Fig. 4 XPS spectra of Ag $3d_{5/2}$ peak of Cpy A (a) and Cpy B (b)

$$7CuFeS_2+8Ag^+ +6O_2=3Cu^{2+}+2Cu_2S+3Ag_2S+ 2Ag^0+7Fe^{2+}+4S^0+2S^{2-}+3SO_4^{2-}+2e \quad (9)$$

3.3.2 XPS spectra of Cu 2p

Figure 5 describes the Cu $2p_{3/2}$ peaks of the residues. For Cpy A (Fig. 5(a)), in both T1 and T2, the Cu $2p_{3/2}$ peaks were observed at 934.39, 932.54 and 931.49 eV, assigning to Cu−O species, Cu in the mineral structure, and Cu in covellite, respectively [37,38]. The appearance of Cu−O species indicated that the chalcopyrite was oxidized. Additionally, it has been declared that the dissolution of covellite-like species is slower than that of chalcopyrite [2]. Therefore, without Ag^+ treatment, the covellite-like species were generated on the surface of the mineral and hindered the dissolution of chalcopyrite. And the surface of chalcopyrite treated with light illumination contained more covellite-like species and less chalcopyrite, indicating that the chalcopyrite was more seriously dissolved and more transformations took place. This was consistent with the results of Figs. 2(a) and (b). While for the residues in T3, the

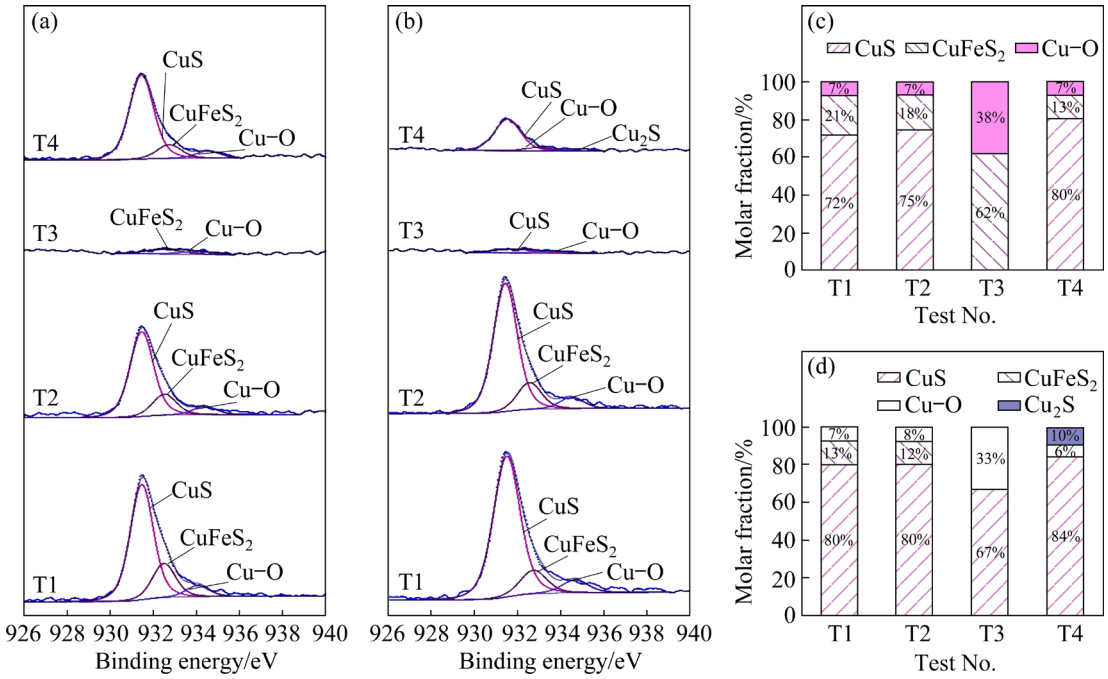

Fig. 5 XPS spectra of Cu $2p_{3/2}$ peaks of Cpy A (a) and CpyB (b) in four tests, and contents of different copper species on surface of Cpy A (c) and CpyB (d)

copper peaks almost disappeared, which indicated that the surface of chalcopyrite was wrapped by other substances. And the remaining few copper peaks were attributed to chalcopyrite and Cu−O species. However, when light illumination and Ag^+ acted together, the copper on the surface of the leached residue was exposed again (the intensity of Cu 2p peak in T4 increased), and further dissolution could occur. Consequently, the highest copper extraction rate was exhibited under the simultaneous presence of light illumination and Ag^+ (Figs. 2(a) and (b)).

For Cpy B (Fig. 5(b)), the evolution of copper on the leached chalcopyrite surface was roughly in keeping with that of Cpy A. However, almost the same contents of chalcopyrite on the surface of leached residues in T1 and T2 implied visible light did not significantly promote the dissolution of Cpy B, which was in agreement with Figs. 2(c) and (d). And the residues in T3 exhibited a small amount of covellite-like (located at 932.9 eV [37,39]) and Cu−O species, while the copper on the surface of leached residues in T4 was primarily composed of covellite-like, Cu−O and chalcocite-like species. Among them, chalcocite-like species could promote the release of copper because its dissolution rate was quicker than that of chalcopyrite [40]. Therefore, light illumination and Ag^+ significantly promoted the dissolution of Cpy B. Moreover, when light illumination and Ag^+ acted simultaneously, the copper content of Cpy B surface was lower than that of Cpy A surface (the peak intensity was weaker), which indicated that the surface of Cpy B was more densely wrapped by other substances. Thus, the copper extraction rate of Cpy A was higher than that of Cpy B.

3.3.3 XPS spectra of S 2p and O 1s

As shown in Fig. 6, the surface sulfur species of two chalcopyrite residues were mainly composed of monosulfide (S^{2-}, 161.1−161.8 eV) [41], elemental sulfur and polysulfide (S^0/S_n^{2-}, 163.1−163.49 eV) [42,43], and sulfate (SO_4^{2-}, 168.5−168.7 eV) [44]. Figure 7 shows the O 1s spectra of leached residues surfaces. The deconvolution of O 1s spectrum listed 3 types of O coordination states present: oxides (O^{2-}, 529.78−530.33 eV) [45], hydroxides (—OH, 530.93−531.4 eV) [42], and sulfate (SO_4^{2-}, 532.2−532.5 eV) [46].

The form of S^{2-} on the surface of samples could be regarded as chalcopyrite [39], while S_n^{2-}, S^0 and SO_4^{2-} were considered as the main components of the passivation layer [29]. Among them, SO_4^{2-} was mainly contributed to jarosite ($KFe_3(SO_4)_2(OH)_6$) and schwertmannite (ideally

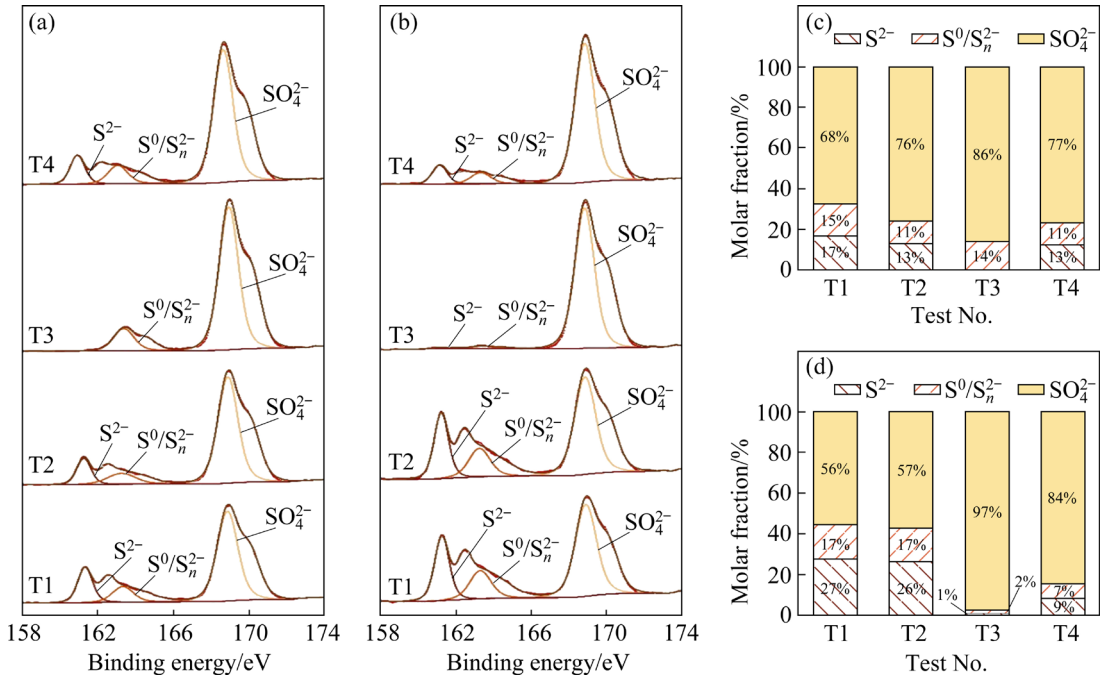

Fig. 6 XPS spectra of S 2p peak (only S $2p_{3/2}$ fitting peaks were displayed) of Cpy A (a) and CpyB (b) in four tests, and contents of different sulfur species on surfaces of Cpy A (c) and CpyB (d)

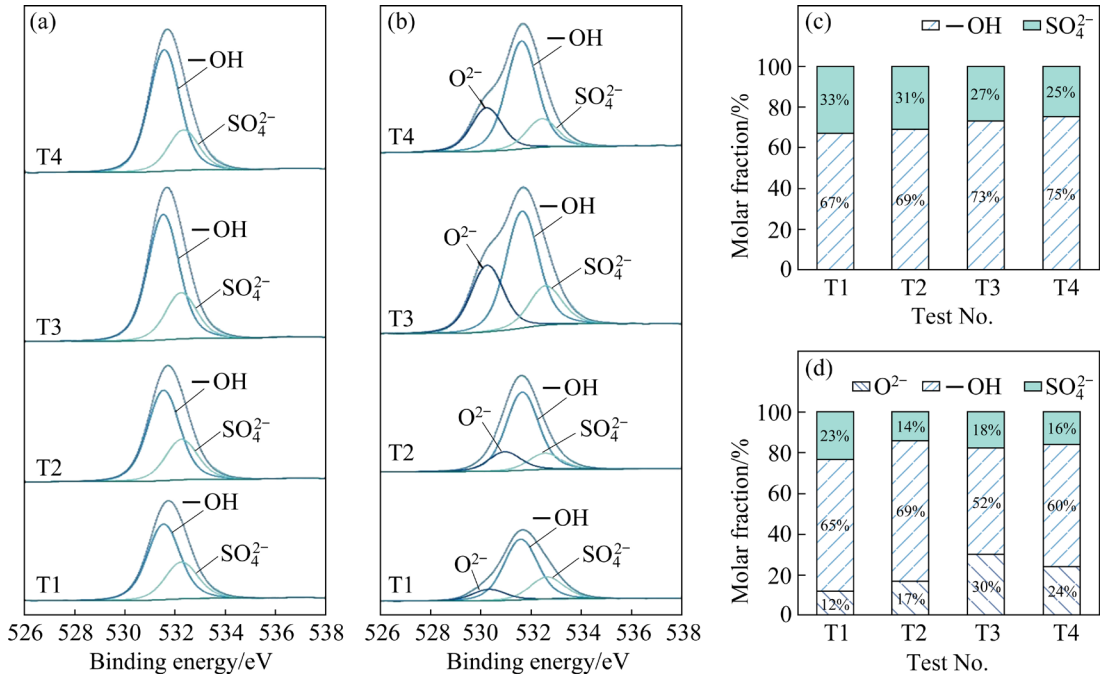

Fig. 7 XPS spectra of O 1s peaks of Cpy A (a) and CpyB (b) in four tests, and contents of diverse oxygen species on surfaces of Cpy A (c) and CpyB (d)

$Fe_8O_8(OH)_6SO_4$), which indicated that the reaction of jarosite formation took place on the chalcopyrite surface (Reaction (10)) [47]. And schwertmannite was a metastable phase with poor crystallinity, which was the solid-phase precursor for jarosite formation in the presence of *A. ferrooxidans* [48]. In all tests, the S species on the chalcopyrite residues surface were dominated by sulfate after bioleaching. Combined with XRD results (Fig. 3), it can be seen that the chalcopyrite on the surface of

leached residues of Cpy A was oxidized to jarosite, while the chalcopyrite on leached Cpy B surface was oxidized to schwertmannite. Furthermore, for the two chalcopyrite samples, the content of sulfate on the surface of leached residues was significantly enhanced after adding Ag^+ (T3 and T4) compared with that without adding Ag^+ (T1 and T2), which meant that Ag^+ markedly accelerated the oxidative dissolution of chalcopyrite. In T2, there was more jarosite than in T1, suggesting that the presence of light accelerated the oxidation of sulfur on the chalcopyrite surface, thereby accelerating copper release. The promotion effect of Cpy A was more obvious, which was also confirmed in Fig. 2. Compared with T3, S^{2-} appeared on the surface of residues in T4, which meant that the chalcopyrite surface was exposed again.

$$M^+ + 3Fe^{3+} + 2SO_4^{2-} + 6H_2O = MFe_3(SO_4)_2(OH)_6 + 6H^+ \quad (10)$$

where M^+ may be K^+, NH_4^+, H_3O^+ or Na^+.

Further, the addition of visible light and Ag^+ increased oxygen content, which indicated that the oxidation degree of the chalcopyrite was increased. However, when visible light and Ag^+ coexist, the peak intensity of O 1s on the surface of residues was slightly weaker than that treated with Ag^+ alone, implying that the content of oxides on the surface of the residues was reduced. The results were also in agreement with the high-resolution narrow spectra of S 2p.

3.4 Surface morphology of leached chalcopyrite

The surface morphologies of Cpy A and Cpy B leached under different conditions are shown in Figs. 8 and 9, respectively. It could be obviously found that the surface of Cpy A in T1 was covered with some nano-sized particles (200−1000 nm), which were speculated as jarosite [49]. Combined with Fig. 3(a), it could be judged that these particles were jarosite. However, the surface of chalcopyrite could still be clearly seen (Fig. 8(a)). The surface of residues in T2 (Fig. 8(b)) was covered with more jarosite than that in T1. In addition to the aggregated jarosite, the surface of chalcopyrite residues in T3 also had some loose and smaller particles (Fig. 8(c)). Moreover, in T4, jarosite on the surface of leached residues was more dispersed (Fig. 8(d)). Jarosite is considered to be the main substance hindering the bioleaching of chalcopyrite because of its insolubility and compactness [50]. Combined with the analysis of Fig. 2, the compactness of jarosite was destroyed after adding Ag^+, especially in the presence of light illumination. Therefore, the blocking effect of jarosite on the dissolution of chalcopyrite was weakened and the release of copper ions was promoted.

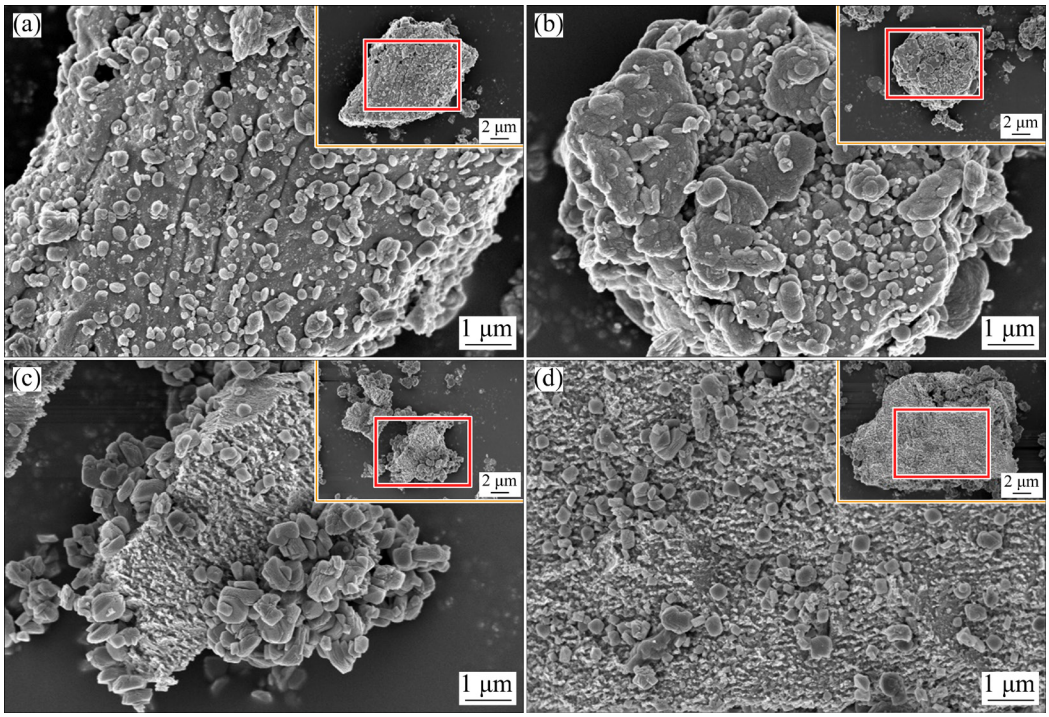

Fig. 8 SEM images of Cpy A in T1 (a), T2 (b), T3 (c) and T4 (d)

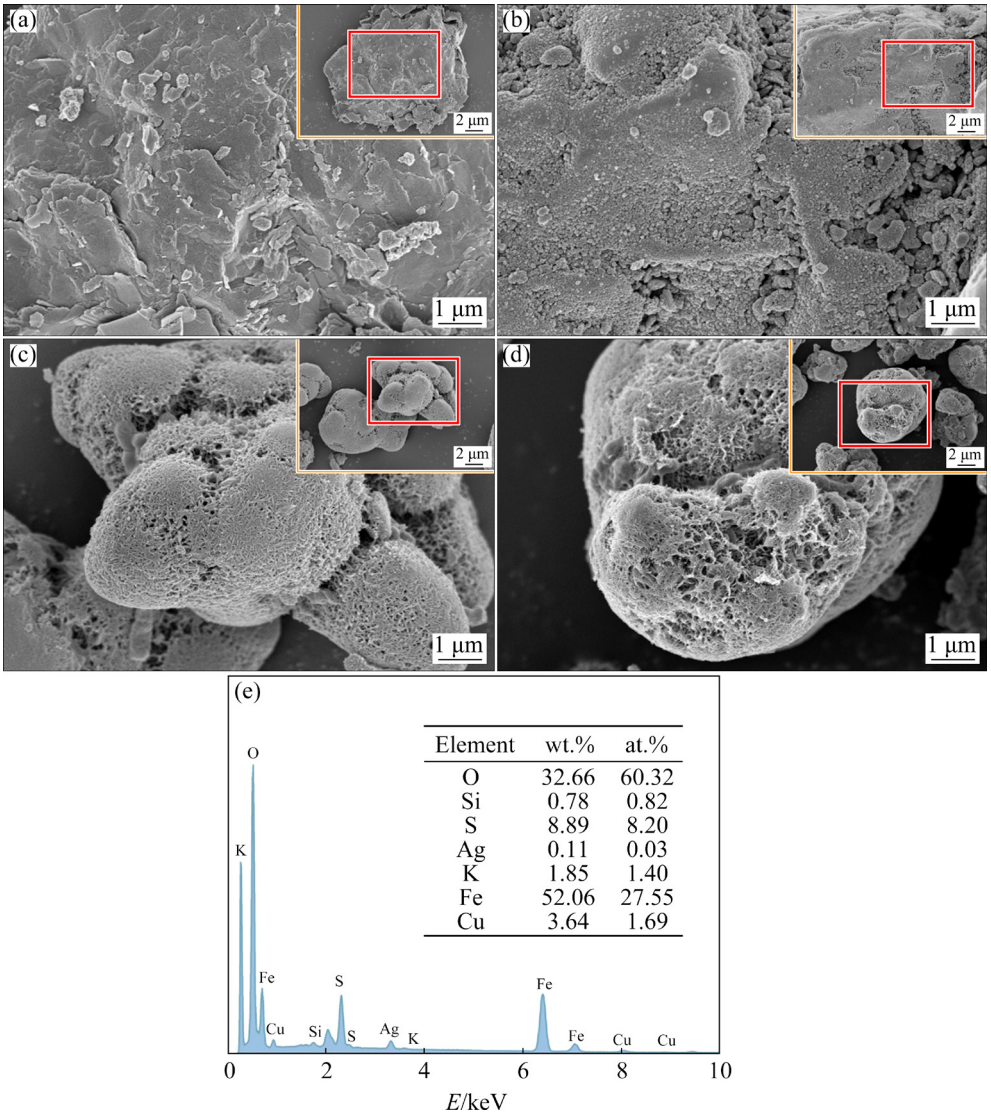

Fig. 9 SEM images of Cpy B in T1 (a), T2 (b), T3 (c) and T4 (d), and contents (e) of surface elements of Cpy B in T3 analyzed by EDS

For Cpy B, however, the surface of leached residues of T1 was relatively smooth, and only some small particles fell off (Fig. 9(a)). The surface of the residue of T2 (Fig. 9(b)) was rougher than that of T1. This indicated that visible light promoted the dissolution of chalcopyrite, which was consistent with the conclusion from Figs. 2(c) and (d). After adding Ag^+, the surface of residues of T3 was wrapped by relatively dense network substances (Fig. 9(c)). Then, the contents of surface elements were examined by EDS (Fig. 9(e)), and combined with the XRD results (Fig. 3(b)) and the high-resolution narrow spectra of S 2p (Fig. 6(b)) of Cpy B, it could be deduced that the network substance was mainly schwertmannite (ideally $Fe_8O_8(OH)_6SO_4$) [51]. When light and Ag^+ were present simultaneously, due to the formation of more Ag_2S (Fig. 4(b)), the dense schwertmannite layer became looser and more porous (Fig. 9(d)), which was conducive to the bioleaching of chalcopyrite. Overall, Cpy A was corroded more seriously than Cpy B in each bioleaching test, which further indicated that Cpy A was easier to dissolve than Cpy B. These results were consistent with Fig. 2.

In summary, it could be inferred that visible light facilitated the generation of Al-bearing species on chalcopyrite surface when Ag^+ was added. Thus, the passivation layer on the mineral surface became loose, and chalcopyrite was exposed, which was conducive to further dissolution. Moreover, the facilitation effect of light illumination and Ag^+ on

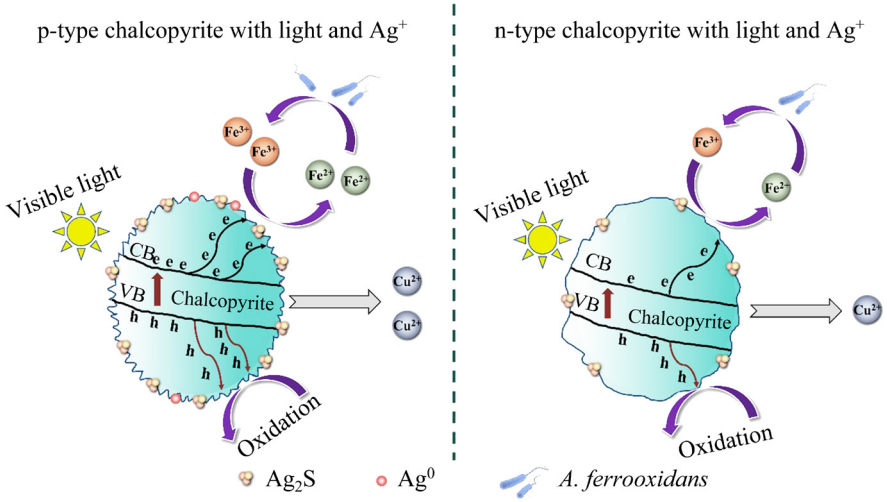

Fig. 10 Different mechanisms of light illumination and Ag^+ accelerating bioleaching of p- and n-type chalcopyrite

Cpy A was more obvious than that on Cpy B (looser surface morphology, more Ag-bearing species, and larger exposed chalcopyrite surface), so the copper extraction rate of Cpy A was higher.

3.5 Mechanism model of p- and n-type chalcopyrite bioleaching

Considering all analysis results in this study, different mechanisms of light illumination and Ag^+ accelerating the bioleaching of different types of chalcopyrite were proposed (Fig. 10). Chalcopyrite has a widely accepted band gap of 0.6 eV with the valence band (VB) and conduction band (CB) [52]. Under the irradiation of visible light, excited electrons jump from VB to CB and generate charge carriers (electron−hole pairs) [24]. Then, electrons and holes migrate to the chalcopyrite surface to promote the reduction and oxidation reactions on the surface of chalcopyrite, respectively [23,25]. Furthermore, the initial reaction in the oxidative dissolution of chalcopyrite is hole consumption, followed by electron migration [33], and the primary carriers of the p-type semiconductor are holes [22]. In this study, since Cpy A (p-type chalcopyrite) had higher carrier concentration and mobility, but lower resistivity than Cpy B (n-type chalcopyrite), the carriers transfer rate of p-type chalcopyrite was faster than that of n-type chalcopyrite, which was conducive to the oxidation−reduction reactions of chalcopyrite, so as to dissolve quickly (Table 1 and Fig. 2). Under the addition of Ag^+, visible light accelerated the charge transfer rate on the surface of chalcopyrite, thus promoting the formation of Ag_2S on the chalcopyrite surface. In particular, due to the higher carrier concentration and mobility of p-type chalcopyrite, the charge transfer rate on its surface was faster than that on the surface of n-type chalcopyrite with light illumination. Therefore, compared with n-type chalcopyrite, in addition to forming more Ag_2S on the surface of p-type chalcopyrite, Ag^0 was also formed. Silver was a very good conductor [53], which could in turn promote the charge transfer on the chalcopyrite surface. Furthermore, the passive film formed on the surface of chalcopyrite became loose as a result of the formation of these Ag-bearing substances, so that chalcopyrite was exposed to the surface, which contributed to further dissolution. Hence, the surface corrosion of p-type chalcopyrite was more serious and released more copper ions when both light illumination and Ag^+ were present.

4 Conclusions

(1) A systematic comparative study using visible light and Ag^+ to catalyze the dissolution of p and n-type chalcopyrite was reported.

(2) Cpy A was p-type chalcopyrite with higher carrier concentration and mobility, and Cpy B belonged to n-type chalcopyrite whose carrier concentration and mobility were lower. Compared with Cpy B, due to the higher carrier concentration and mobility, the higher solubility and stronger response to the light illumination of Cpy A were achieved.

(3) Under visible light illumination, Ag^+ introduced more Ag-bearing substances (Ag_2S and

Ag^0) on the surface of Cpy A, so the surface of Cpy A was rougher and looser than that of Cpy B, and larger chalcopyrite surface was exposed, which was favorable for further dissolution. Therefore, under the action of Ag^+ together with visible light, the copper extraction rate of Cpy A was remarkably higher than that of Cpy B.

CRediT authorship contribution statement

Chun-xiao ZHAO: Investigation, Data analysis, Interpretation of results, Writing − Original draft; **Jun WANG:** Resources, Funding acquisition, Project administration; **Yang LIU:** Writing − Review & editing, Project administration; **Rui LIAO:** Writing − Review & editing; **Bao-jun YANG:** Investigation, Writing − Review & editing; **Guan-zhou QIU:** Resources, Conceptualization.

Declaration of competing interest

The authors declare that they have no known competing financial interests or personal relationships that could have appeared to influence the work reported in this paper.

Acknowledgments

The authors are grateful for the financial supports from the National Key Research and Development Program of China (No. 2022YFC2105300), and the National Natural Science Foundation of China (Nos. 52274288, 51934009, 52204303).

References

[1] DONG Zhong-lin, JIANG Tao, XU Bin, ZHONG Hong, ZHANG Bang-sheng, LIU Gui-qing, LI Qian, YANG Yong-bin. Density functional theory study on electronic structure of tetrahedrite and effect of natural impurities on its flotation property [J]. Minerals Engineering, 2021, 169: 106980.

[2] XIA Jin-lan, SONG Jian-jun, LIU Hong-chang, NIE Zhen-yuan, SHEN Li, YUAN Peng, MA Chen-yan, ZHENG Lei, ZHAO Yi-dong. Study on catalytic mechanism of silver ions in bioleaching of chalcopyrite by SR-XRD and XANES [J]. Hydrometallurgy, 2018, 180: 26−35.

[3] ZENG Wei-min, PENG Yu-ping, PENG Tang-jian, NAN Mei-hua, CHEN Miao, QIU Guan-zhou, SHEN Li. Electrochemical studies on dissolution and passivation behavior of low temperature bioleaching of chalcopyrite by *Acidithiobacillus ferrivorans* YL15 [J]. Minerals Engineering, 2020, 155: 106416.

[4] KHAING S Y, SUGAI Y, SASAKI K. Gold dissolution from ore with iodide-oxidising bacteria [J]. Scientific Reports, 2019, 9(1): 4178.

[5] ZHAO Hong-bo, ZHANG Yi-sheng, ZHANG Xian, QIAN Lu, SUN Meng-lin, YANG Yu, ZHANG Yan-sheng, WANG Jun, KIM H, QIU Guan-zhou. The dissolution and passivation mechanism of chalcopyrite in bioleaching: An overview [J]. Minerals Engineering, 2019, 136: 140−154.

[6] WANG Yu-guang, ZENG Wei-min, QIU Guan-zhou, CHEN Xin-hua, ZHOU Hong-bo. A moderately thermophilic mixed microbial culture for bioleaching of chalcopyrite concentrate at high pulp density [J]. Applied and Environmental Microbiology, 2014, 80: 741−750.

[7] EBRAHIMPOUR S, ABDOLLAHI H, GHARABAGHI M, MANAFI Z, TUOVINEN O H. Acid bioleaching of copper from smelter dust at incremental temperatures [J]. Mineral Processing and Extractive Metallurgy Review, 2022, 43(2): 233−242.

[8] ABDOLLAHI H, NOAPARAST M, SHAFAEI S Z, MANAFI Z, MUÑOZ J A, TUOVINEN O H. Silver-catalyzed bioleaching of copper, molybdenum and rhenium from a chalcopyrite−molybdenite concentrate [J]. International Biodeterioration & Biodegradation, 2015, 104: 194−200.

[9] ABDOLLAHI H, SHAFAEI S Z, NOAPARAST M, MANAFI Z, NIEMELÄ S I, TUOVINEN O H. Mesophilic and thermophilic bioleaching of copper from a chalcopyrite-containing molybdenite concentrate [J]. International Journal of Mineral Processing, 2014, 128: 25−32.

[10] ABDOLLAHI H, SHAFAEI S Z, NOAPARAST M, MANAFI Z, ASLAN N. Bio-dissolution of Cu, Mo and Re from molybdenite concentrate using mix mesophilic microorganism in shake flask [J]. Transactions of Nonferrous Metals Society of China, 2013, 23: 219−230.

[11] ZHANG Yu, ZHANG Shuang, ZHAO Dan, NI Yong-qing, WANG Wei-dong, LEI Yan. Complete genome sequence of *Acidithiobacillus ferrooxidans* YNTRS-40, a strain of the ferrous iron- and sulfur-oxidizing acidophile [J]. Microorganisms, 2019, 8(1): 2.

[12] QUATRINI R, JOHNSON D B. *Acidithiobacillus ferrooxidans* [J]. Trends in Microbiology, 2019, 27(3): 282−283.

[13] SU Gui-rong, DENG Xiao-tao, ZHONG Hui, HU Liang, LI Shu-zhen, PRABURAMAN L, HE Zhi-guo, SUN Wei. Ag^+ significantly promoted the biofilm formation of thermoacidophilic archaeon *Acidianus manzaensis* YN-25 on chalcopyrite surface [J]. Chemosphere, 2021, 276: 130208.

[14] MILLER J D, MCDONOUGH P J, PORTILLO H Q. Electrochemistry in silver catalyzed ferric sulfate leaching of chalcopyrite [J]. Electrochemical Reactions and Solution Chemistry, 1981, 27: 327−338.

[15] PRICE D W, WARREN G W. The influence of silver ion on the electrochemical response of chalcopyrite and other mineral sulfide electrodes in sulfuric acid [J]. Hydrometallurgy, 1986, 15: 303−324.

[16] GHAHREMANINEZHAD A, RADZINSKI R, GHEORGHIU T, DIXON D G, ASSELIN E. A model for silver ion catalysis of chalcopyrite ($CuFeS_2$) dissolution [J]. Hydrometallurgy, 2015, 155: 95−104.

[17] O'CONNOR G M, EKSTEEN J J. A critical review of the passivation and semiconductor mechanisms of chalcopyrite leaching [J]. Minerals Engineering, 2020, 154: 106401.

[18] WEN Ting, WANG Yong-gang, LI Na-na, ZHANG Qian,

ZHAO Yong-sheng, YANG Wen-ge, ZHAO Yu-sheng, MAO Ho-kwang. Pressure-driven reversible switching between n- and p-type conduction in chalcopyrite $CuFeS_2$ [J]. Journal of the American Chemical Society, 2019, 141(1): 505−510.

[19] HUANG Xiao-tao, ZHU Tong-he, DUAN Wei-jian, LIANG Sheng, LI Ge, XIAO Wei. Comparative studies on catalytic mechanisms for natural chalcopyrite-induced Fenton oxidation: Effect of chalcopyrite type [J]. Journal of Hazardous Materials, 2020, 381: 120998.

[20] ZHAO Hong-bo, HUANG Xiao-tao, WANG Jun, LI Yi-ni, LIAO Rui, WANG Xing-xing, QIU Xiao, XIONG Yu-ming, QIN Wen-qing, QIU Guan-zhou. Comparison of bioleaching and dissolution process of p-type and n-type chalcopyrite [J]. Minerals Engineering, 2017, 109: 153−161.

[21] VALDOVINOS S M, GUREVICH Y G. Hall effect: the role of nonequilibrium charge carriers [J]. Revista Mexicana De Fisica, 2011, 57(4): 368−374.

[22] MOBARAK M, NASSARY M M, GAMI F, MOSTAFA M. Growth and transport properties of $AgInS_2$ ternary semiconductor [J]. Journal of Materials Science: Materials in Electronics, 2022, 33(13): 10278−10286.

[23] YEPSEN O, YANEZ J, MANSILLA H D. Photocorrosion of copper sulfides: Toward a solar mining industry [J]. Solar Energy, 2018, 171: 106−111.

[24] CRUNDWELL F K, BRYSON L J, ASWEGEN A V, KNIGHTS B D H. Effect of chopped light on the dissolution and leaching of chalcopyrite [J]. Minerals Engineering, 2021, 160: 106703.

[25] ZHOU Shuang, GAN Min, ZHU Jian-yu, LI Qian, JIE Shi-qi, YANG Bao-jun, LIU Xue-duan. Catalytic effect of light illumination on bioleaching of chalcopyrite [J]. Bioresource Technology, 2015, 182: 345−352.

[26] ZHAO Chun-xiao, YANG Bao-jun, LIAO Rui, HONG Mao-xin, YU Shi-chao, LIU Shi-tong, WANG Jun, QIU Guan-zhou. Combined effect and mechanism of visible light and Ag^+ on chalcopyrite bioleaching [J]. Minerals Engineering, 2022, 175: 107283.

[27] SU Jian-wei, YANG Yang, XIA Guo-liang, CHEN Ji-tang, JIANG Peng, CHEN Qian-wang. Ruthenium−cobalt nanoalloys encapsulated in nitrogen-doped graphene as active electrocatalysts for producing hydrogen in alkaline media [J]. Nature Communications, 2017, 8: 14969.

[28] PANOSSIAN Z, FERRARI J V, ALMEIDA M B. Determination of copper and zinc contents in brass plating solutions by titrimetric analysis: A review [J]. Plating & Surface Finishing, 2004, 91: 38−43.

[29] YANG Bao-jun, ZHAO Chun-xiao, LUO Wen, LIAO Rui, GAN Min, WANG Jun, LIU Xue-duan, QIU Guan-zhou. Catalytic effect of silver on copper release from chalcopyrite mediated by *Acidithiobacillus ferrooxidans* [J]. Journal of Hazardous Materials, 2020, 392: 122290.

[30] PENG Tang-jian, LIAO Wan-qing, WANG Jing-shu, MIAO Jie, PENG Yu-ping, GU Guo-hua, WU Xue-ling, QIU Guan-zhou, ZENG Wei-min. Bioleaching and electrochemical behavior of chalcopyrite by a mixed culture at low temperature [J]. Frontiers in Microbiology, 2021, 12: 663757.

[31] ZHAO Chun-xiao, YANG Bao-jun, WANG Xing-xing, ZHAO Hong-bo, GAN Min, QIU Guan-zhou, WANG Jun. Catalytic effect of visible light and Cd^{2+} on chalcopyrite bioleaching [J]. Transactions of Nonferrous Metals Society of China, 2020, 30(4): 1078−1090.

[32] DROGUETT C, SALAZAR R, BRILLAS E, SIRES I, CARLESI C, MARCO J F, THIAM A. Treatment of antibiotic cephalexin by heterogeneous electrochemical Fenton-based processes using chalcopyrite as sustainable catalyst [J]. Science of the Total Environment, 2020, 740: 140154.

[33] LI Hong-xu, WANG Dian-zuo. Fundamental analysis of sulfide bioleaching process based on semiconductor electrochemistry [J]. Nonferrous Metals, 2004, 56(3): 35−37. (in Chinese)

[34] HUANG Dan-yu, CHEN Ning, ZHU Chang-yin, FANG Guo-dong, ZHOU Dong-mei. The overlooked oxidative dissolution of silver sulfide nanoparticles by thermal activation of persulfate: Processes, mechanisms, and influencing factors [J]. Science of the Total Environment, 2021, 760: 144504.

[35] LAL S S, MHASKE S T. AgBr and AgCl nanoparticle doped TEMPO-oxidized microfiber cellulose as a starting material for antimicrobial filter [J]. Carbohydrate Polymers, 2018, 191: 266−279.

[36] TAPERA T, NIKOLOSKI A N. The effect of silver on the acidic ferric sulfate leaching of primary copper sulfides under recycle solution conditions observed in heap leaching. Part 4: Semiconductor behaviour [J]. Hydrometallurgy, 2019, 186: 50−57.

[37] TIAN Xiao-dong, LI Xue-ting, BI Peng-fei. Effect of O-isobutyl-N-ethyl thionocarbamates on flotation behavior of porphyry copper ore and its adsorption mechanism [J]. Applied Surface Science, 2020, 503: 144313.

[38] WU Hai-bin, OR V W, GONZALEZ-CALZADA S, GRASSIAN V H. CuS nanoparticles in humid environments: Adsorbed water enhances the transformation of CuS to $CuSO_4$ [J]. Nanoscale, 2020, 12: 19350−19358.

[39] WANG Jun, GAN Xiao-wen, ZHAO Hong-bo, HU Ming-hao, LI Kai-yun, QIN Wen-qing, QIU Guan-zhou. Dissolution and passivation mechanisms of chalcopyrite during bioleaching: DFT calculation, XPS and electrochemistry analysis [J]. Minerals Engineering, 2016, 98: 264−278.

[40] HIROYOSHI N, ARAI M, MIKI H, TSUNEKAWA M, HIRAJIMA T. A new reaction model for the catalytic effect of silver ions on chalcopyrite leaching in sulfuric acid solutions [J]. Hydrometallurgy, 2002, 63: 257−267.

[41] BAI Yun-long, WANG Wei, ZHAO Shan-rong, LU Dian-kun, XIE Feng, DREISINGER D. Effect of mechanical activation on leaching behavior and mechanism of chalcopyrite [J]. Mineral Processing and Extractive Metallurgy Review, 2021, 43(4): 440−452.

[42] YUAN Duo-wei, CADIEN K, LIU Qi, ZENG Hong-bo. Adsorption characteristics and mechanisms of O-carboxymethyl chitosan on chalcopyrite and molybdenite [J]. Journal of Colloid and Interface Science, 2019, 552: 659−670.

[43] JIA Yuan, HUANG Xiao-ping, CAO Zhan-fang, WANG Shuai, ZHONG Hong. Investigation on the selectivity of thioamide surfactants and adsorption mechanism of thio-p-

toluamide for chalcopyrite [J]. Applied Surface Science, 2019, 484: 864−875.
[44] NIE Qing-min, WANG Meng-yu, QIU Ting-sheng, QIU Xian-hui. Density functional theory and XPS studies of the adsorption of cyanide on chalcopyrite surfaces [J]. ACS Omega, 2020, 5(36): 22778−22785.
[45] HUANG Xiao-ping, HUANG Kai-hua, WANG Shuai, CAO Zhan-fang, ZHONG Hong. Synthesis of 2-hydroxyethyl dibutyldithiocarbamate and its adsorption mechanism on chalcopyrite [J]. Applied Surface Science, 2019, 476: 460−467.
[46] KHOSO S A, GAO Zhi-yong, TIAN Meng-jie, HU Yue-hua, SUN Wei. Adsorption and depression mechanism of an environmentally friendly reagent in differential flotation of Cu−Fe sulphides [J]. Journal of Materials Research and Technology, 2019, 8(6): 5422−5431.
[47] ZHAO Chun-xiao, YANG Bao-jun, LIAO Rui, HONG Mao-xin, YU Shi-chao, WANG Jun, QIU Guan-zhou. Catalytic mechanism of manganese ions and visible light on chalcopyrite bioleaching in the presence of *Acidithiobacillus ferrooxidans* [J]. Chinese Journal of Chemical Engineering, 2022, 41: 457−465.
[48] WATLING H R, ELLIOT A D, MALEY M, BRONSWIJK W V, HUNTER C. Leaching of a low-grade, copper−nickel sulfide ore. 1: Key parameters impacting on Cu recovery during column bioleaching [J]. Hydrometallurgy, 2009, 97: 204−212.
[49] YANG Bao-jun, LIN Mo, FANG Jing-hua, ZHANG Rui-yong, LUO Wen, WANG Xing-xing, LIAO Rui, WU Bai-qiang, WANG Jun, GAN Min, LIU Bin, ZHANG Yi, LIU Xue-duan, QIN Wen-qing, QIU Guan-zhou. Combined effects of jarosite and visible light on chalcopyrite dissolution mediated by *Acidithiobacillus ferrooxidans* [J]. Science of the Total Environment, 2020, 698: 134175.
[50] LIAO Rui, YANG Bao-jun, HUANG Xiao-tao, HONG Mao-xing, YU Shi-chao, LIU Shi-tong, WANG Jun, QIU Guan-zhou. Combined effect of silver ion and pyrite on AMD formation generated by chalcopyrite bio-dissolution [J]. Chemosphere, 2021, 279: 130516.
[51] MUKHERJEE C, JONES F S, BIGHAM J M, TUOVINEN O H. Synthesis of argentojarosite with simulated bioleaching solutions produced by *Acidithiobacillus ferrooxidans* [J]. Materials Science and Engineering C, 2016, 66: 164−169.
[52] CRUNDWELL F K. The semiconductor mechanism of dissolution and the pseudo-passivation of chalcopyrite [J]. Canadian Metallurgical Quarterly, 2015, 54(3): 279−288.
[53] AL-MILAJI K N, HUANG Qi-jin, LI Zhen, NG T N, ZHAO Hong. Direct embedment and alignment of silver nanowires by inkjet printing for stretchable conductors [J]. ACS Applied Electronic Materials, 2020, 2(10): 3289−3298.

可见光和银离子对 p 型和 n 型黄铜矿生物浸出的影响机理

赵春晓，王 军，刘 洋，廖 蕤，杨宝军，邱冠周

中南大学 资源加工与生物工程学院 生物冶金教育部重点实验室，长沙 410083

摘 要：研究可见光和银离子(Ag^+)对嗜酸氧化亚铁硫杆菌浸出 p 型和 n 型黄铜矿(黄铜矿 A 和黄铜矿 B)的不同影响及机理。通过霍尔效应试验、生物浸出试验、X 射线衍射、扫描电子显微镜和 X 射线光电子能谱对黄铜矿的半导体性质、生物浸出行为、表面形貌、主要物相和表面物种进行分析。实验结果表明，黄铜矿 A 比黄铜矿 B 具有更高的载流子浓度和更大的载流子迁移率，因此其溶出速率更快。生物浸出 24 d 后，当光照和 Ag^+同时存在时，黄铜矿 A 的铜浸出率为 91.05%，比黄铜矿 B 的铜浸出率(73.19%)高 17.86%。显然，可见光和 Ag^+对黄铜矿 A 生物溶解过程的促进作用强于黄铜矿 B，这主要归因于黄铜矿 A 具有更高的载流子迁移率。此外，在光照影响下，黄铜矿表面电荷转移加快，导致 Ag_2S 积累增多(特别是黄铜矿 A)，从而导致钝化层致密结构被破坏，钝化效果降低，黄铜矿溶解加速。

关键词：嗜酸氧化亚铁硫杆菌；霍尔效应；半导体性质；光照；黄铜矿；生物浸出

(Edited by Wei-ping CHEN)